Journal of Magnetic Resonance **156,** 1–9 (2002)
doi:10.1006/jmre.2002.2532

Short Planar Gradient Coils for MR Microscopy Using Concentric Return Paths

Stephen J. Dodd[1] and Chien Ho[2]

Pittsburgh NMR Center for Biomedical Research and Department of Biological Sciences, Carnegie Mellon University, Pittsburgh, Pennsylvania 15213

Received July 25, 2001; revised March 15, 2002; published online May 31, 2002

The aim of this work is to design a set of gradient coils with an optimal geometry for magnetic resonance microscopy studies. Designs for a three-axis gradient coil system particularly suited for studies with small radiofrequency coils are presented. The novel geometry involves a planar section with concentric return paths to keep the coil short. Reduction of the external field has been attempted by varying the positions of the return paths using a simulated annealing algorithm. A biplanar version of x- and z-directed prototype gradients was built and tested. A 2D-MR image of a grid phantom has been obtained on a 7-T MR instrument to demonstrate the theory. A three-axis set used as a surface gradient set has also been built and used to obtain high-resolution MR images. © 2002 Elsevier Science (USA)

Key Words: **magnetic resonance microscopy; gradient design; RF microcoil; surface gradient; simulated annealing.**

INTRODUCTION

It is well known that one of the features required to obtain high-resolution images with magnetic resonance (MR) is the ability to generate very high magnetic field gradient strengths. Conventionally, gradient coils use a cylindrical geometry that generates restrictions on sample geometry and access, necessitated by the small gradient sets needed to produce high gradient strengths. These cylindrical gradient geometries enforce strict limitations on the dimensions of the sample and are not optimal for the highly sensitive solenoid radiofrequency (RF) coil, a favored design for MR microscopy studies. Quadrupolar gradient coils are very suitable for solenoid RF coils and have been used successfully for high gradient strength imaging and diffusion measurements, although also limiting the sample to being cylindrical (*1*).

A major concern with cylindrical geometries is the length of the gradient coil, compared to its diameter, inhibiting access to samples in microscopy studies. The use of concentric return paths provides an effective method for reducing the length (*2–4*). However, this geometry is still not optimal for the MR microscopy studies, particularly for the small samples involved. For the study of histological samples on microscope slides, planar gradient coils are the obvious solution for an optimal filling factor. The use of a planar geometry also allows the use of solenoidal RF coils without placing length restrictions on the sample, creating easier sample preparation. This will also enable the high gradient strengths necessary for MR microscopy as these gradients coils may be placed as close as necessary to the sample.

Presented here are designs for 3-axis gradient sets which allow easy access for microscope slide samples and for cylindrical samples and have been designed specifically for use with RF microcoils, either solenoids or planar surface coils. The design method takes into account only the gradient strength with the assumption that with the large size of the gradient compared to the sample, the basic geometry will provide a large enough imaging region. The designs incorporate previous work carried out in our laboratory along with further developments. The use of such small RF coils is known to increase the sensitivity of the NMR experiment (*5*, *6*). The design uses concentric return paths similar to designs previously mentioned to keep the gradient set short, but with a planar section to provide an optimal geometry for generating high gradient strengths. These gradients may be used either as a biplanar gradient set or as surface gradients (i.e., one-half of a biplanar set). The return paths may be adjusted to reduce the field external to the gradient coils for use in small-bore magnets and is a possible alternative to planar microgradient designs for vertical bore magnets provided by Seeber *et al.* (*7*).

DESIGN METHOD

A simulated annealing algorithm, an established gradient optimization procedure (*8*), was used to generate the coil designs. Gradient field considerations for the error function only take into account the gradient strength near the origin. This was calculated using Biot–Savart summations, with the coil loops split into 100 sections. It was reasoned that once a basic coil geometry was chosen for each gradient direction, then gradient strength was of primary importance and that if the sample or RF coil was small enough, the gradient would be linear over the region of interest. The shape of the return paths is somewhat arbitrary, but here it has been chosen to fit around a cylinder.

[1] Present address: Research Imaging Center, University of Texas Health Science Center at San Antonio, 8403 Floyd Curl Drive, San Antonio, TX 78229.

[2] To whom correspondence should be addressed at Department of Biological Sciences, Carnegie Mellon University, Pittsburgh, PA 15213. E-mail: chienho@andrew.cmu.edu.

1090-7807/02 $35.00

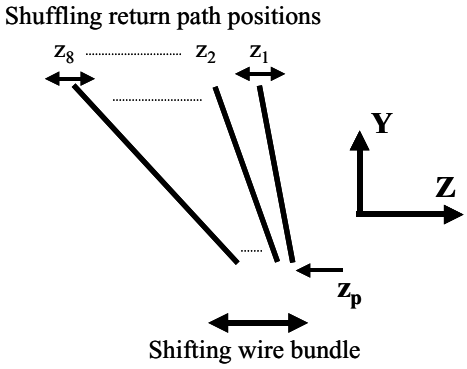

FIG. 1. Scheme for positional adjustments in the simulated annealing algorithm.

To keep the design very simple and buildable, each half of the planar coil section was limited to one layer of wires with the distance between these adjustable. The distance between the gradient halves is kept constant. Reduction of the external field has been attempted by adjusting the current density of the return paths through positional changes. The error function, E, is simply of the form

$$E = \frac{1}{G_{\mathrm{AV}}} + \sum_k B_{\mathrm{sh}}(k)^2, \qquad [1]$$

where G_{AV} is the average gradient at a few points near the origin, and B_{sh} is the z-component of the magnetic field used for the shielding value. Coils were limited to 16 turns in each half of the coil. The algorithm adjusted wire positions in the manner shown in Fig. 1. The return path positions are shuffled independently of each other, and the primary section of the coil is shifted as a bundle. The "temperature" variable of the annealing algorithm was reduced by 10% for a maximum of 50 temperatures. Fifty coil adjustments were performed at each temperature. The extent of the random positional changes was reduced by 5% along with "temperature" changes. The optimization takes approximately 1 min on a 1-GHz PC. Resistance calculations were performed by calculation of the length of the wire and known data for copper resistivity and wire cross section. The torque on each half of the coil was calculated using summations similar to the Biot–Savart method using

$$d\tau = i\, dl \times B, \qquad [2]$$

where $d\tau$ is the elemental torque contribution from segment dl, i is the current, and B is the external field.

RESULTS

Numerical Simulations

Biplanar Gradients

Figure 2A shows an example of a shielded biplanar x-gradient design. The numerical simulations indicate a usable linear region (defined to be a 5% tolerance from the central value) of approximately 2 mm in diameter through the central planes of the gradient, shown in Figs. 2B and 2C. This can be considered sufficient for studies using RF microcoils. The calculated gradient strength for this arrangement is 130 mT/m at the center of the coil, with the separation of the planes being 6.6 mm. The radii of the return paths are 10 mm, and the wire diameter used for these simulations is 0.4 mm. This was compared with an unshielded coil, in which the return paths do not spread out, which produced a gradient strength of 85 mT/m/A (see Table 1). The results obtained for the z- and y-gradients are shown in Figs. 3 and 4. The calculated z-gradient strength is 274 mT/m/A with the plane separation being 6.6 mm. The y-gradient strength is 272 mT/m/A with a plane separation 6.6 mm. Unshielded designs provide calculated strengths of 269 mT/m/A and 232 mT/m/A for z- and y-gradients, respectively (Table 1). Wire positions for the coil designs are given in Table 2.

TABLE 1
Gradient Efficiencies (mT m^{-1} A^{-1}) for Unshielded and Shielded Designs at a Plane Separation of 6.6 mm

	x-gradient (mT m^{-1} A^{-1})	y-gradient (mT m^{-1} A^{-1})	z-gradient (mT m^{-1} A^{-1})
Unshielded design	85	232	269
Shielded design	130	272	274

For all the biplanar gradient designs, the residual field outside the coil has been calculated only at one radial position, at $x = 0$, and 5 mm outside the shield (i.e., $y = 1.5$ mm) and out to 50 mm in the z-direction, for the y- and z-gradients. For the x-gradient, this position is still at 5 mm outside the shield but at a 45° offset. In order to determine the effect of the shielding calculation, the resultant design is compared with the unshielded design, such as in Fig. 5A for a y-gradient design. The field is calculated parallel to the z-axis and at 5 mm from the return paths. The root-mean-square (rms) value of the z-component of the magnetic field for the shielded design was reduced to approximately 20% of that for the unshielded design, as shown in Fig. 5B. For the

TABLE 2
Wire Positions for Each Gradient with the Arrangement from Fig. 1

	x-gradient	y-gradient	z-gradient
zp	0.0	0.0	1.6
z1	0.849	0.219	1.45
z2	2.92	0.679	1.85
z3	3.65	1.09	2.29
z4	6.53	3.72	4.43
z5	6.69	6.68	7.13
z6	7.01	9.6	10.03
z7	8.91	12.5	13
z8	9.79	15.5	15.9

Note. The positions are for the gradient shown in Figs. 2–4.

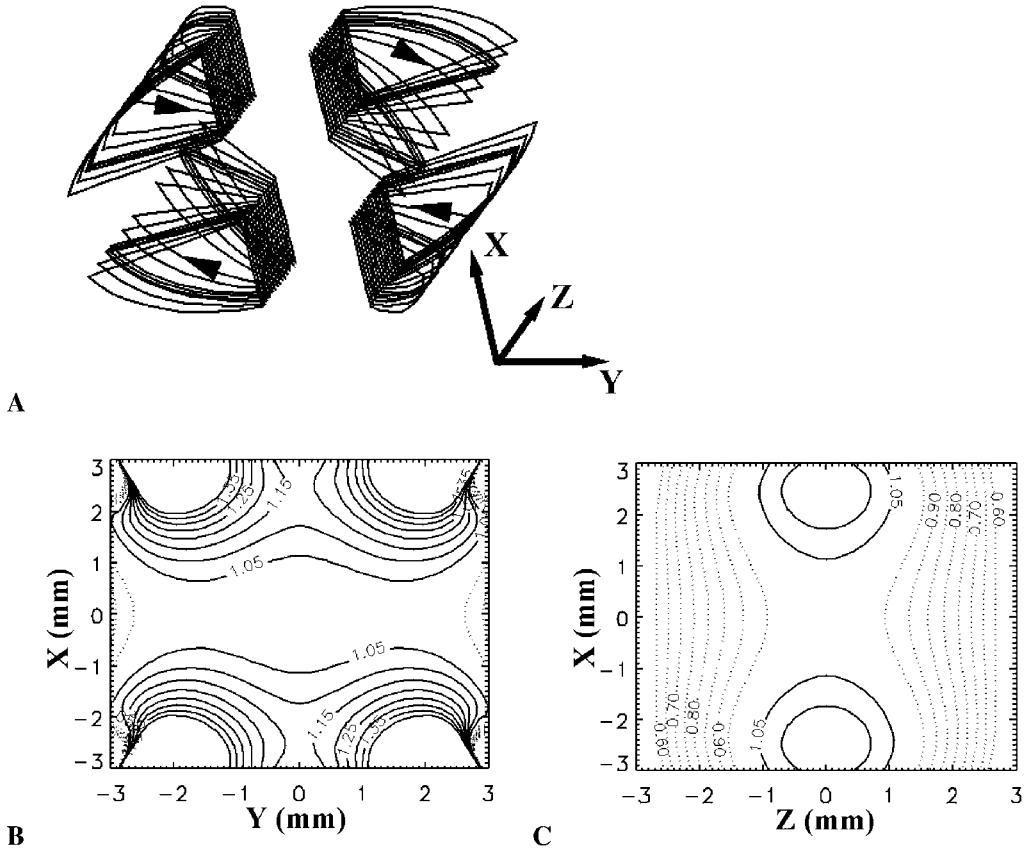

FIG. 2. (A) An example of a resultant x-gradient design. Arrows indicate the current direction in each quadrant. (B) A contour plot showing deviations in field linearity from the central value in the x-y plane in levels of 5%. (C) A contour plot for the x-z plane.

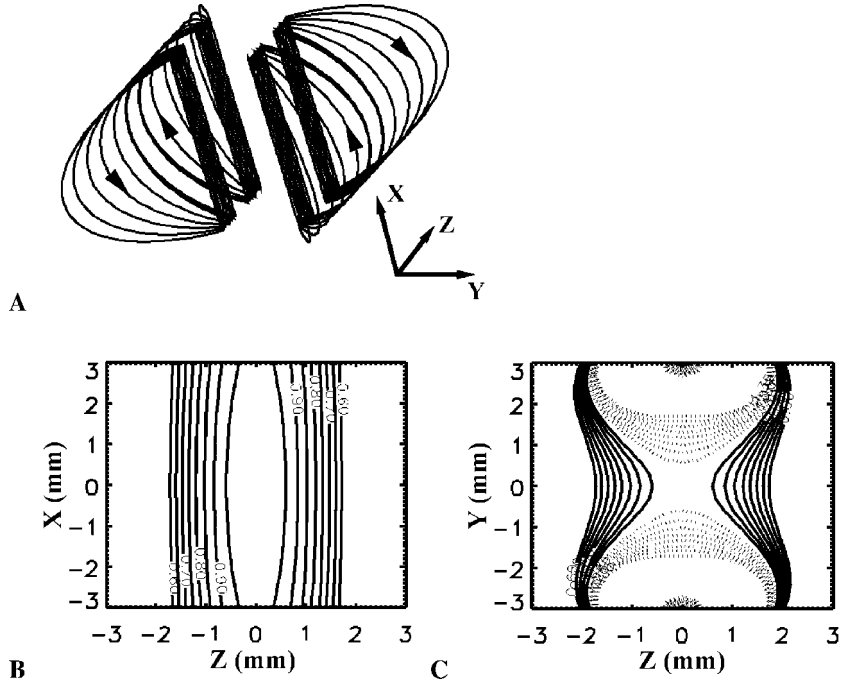

FIG. 3. (A) An example of a resultant z-gradient design. Arrows indicate the current direction. (B) A contour plot showing deviations in field linearity from the central value in the x-z plane. (C) A contour plot for the y-z plane.

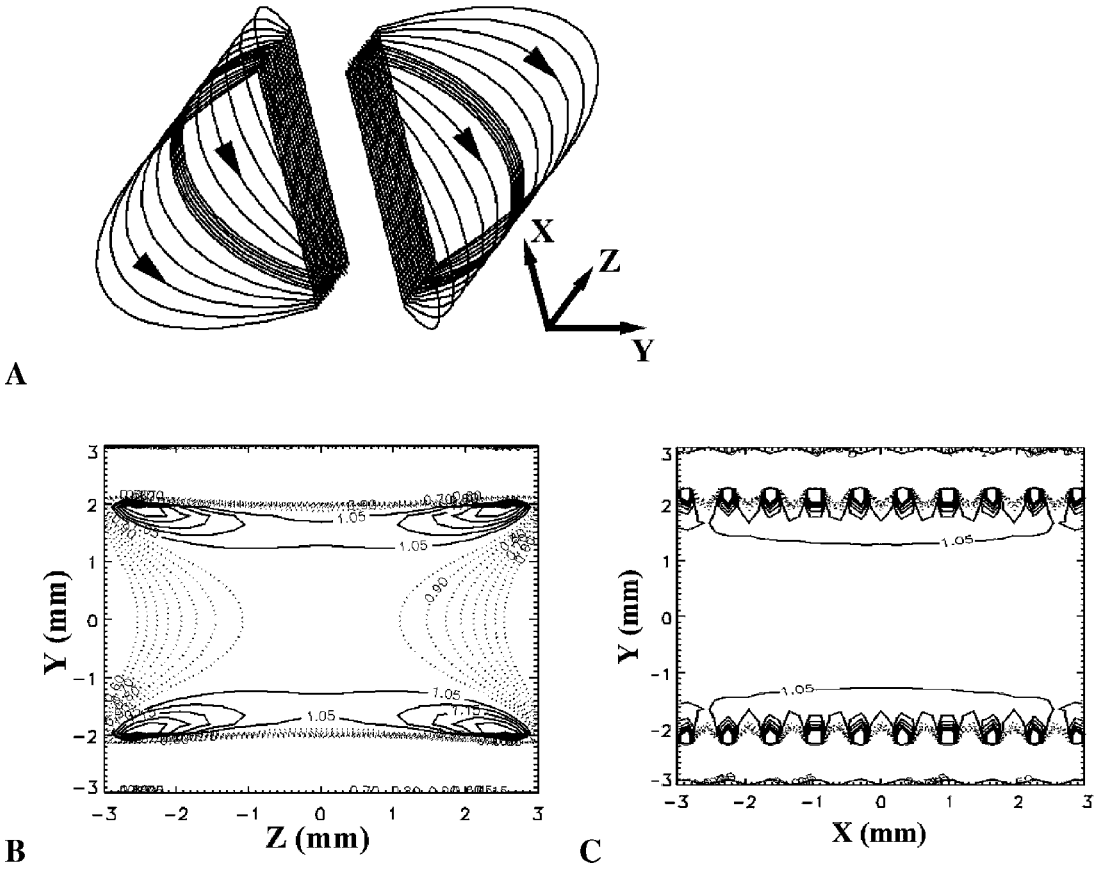

FIG. 4. (A) An example of a resultant y-gradient design. Arrows indicate the current direction. (B) A contour plot showing deviations in field linearity from the central value in the y-z plane. (C) A contour plot for the x-y plane.

x-gradient, the residual field was reduced to 33% at the position used in the coil optimization algorithm. The shielding is less effective for the z-gradient due to the close proximity of the opposing current direction paths producing a canceling effect in the return paths. The value of the external field was 90% of that for the unshielded position. Neglecting the circular return paths for this gradient all together results in a lower residual field.

To determine if the single line calculation for the shielding is appropriate, the rms field value has been calculated at other radial positions outside the coil. Figure 6A shows the results of these calculations for a y-gradient design. It can be seen that the rms field value remains fairly constant for the shielded version and becoming zero at the cancellation point between the two planes. This characteristic justifies the use of the single line calculation

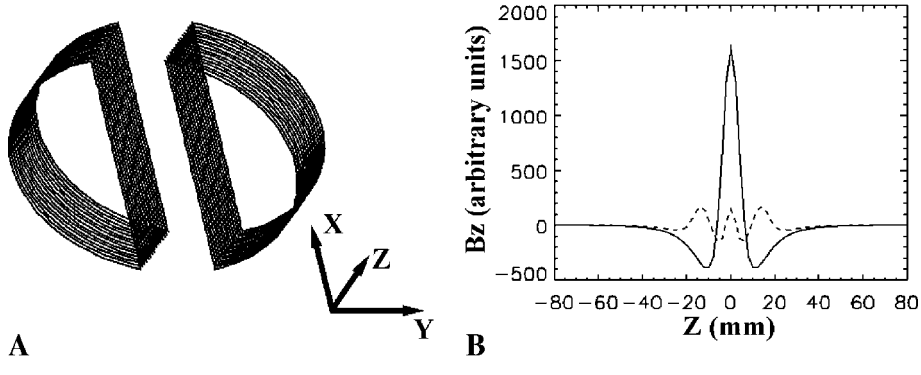

FIG. 5. (A) An unshielded version of the y-gradient and (B) the magnetic field profile 5 mm outside the return paths, at $x = 0$ for both the shielded and unshielded designs. The dotted line represents the shielded version. The rms value of the shielded field was 20% of the unshielded value.

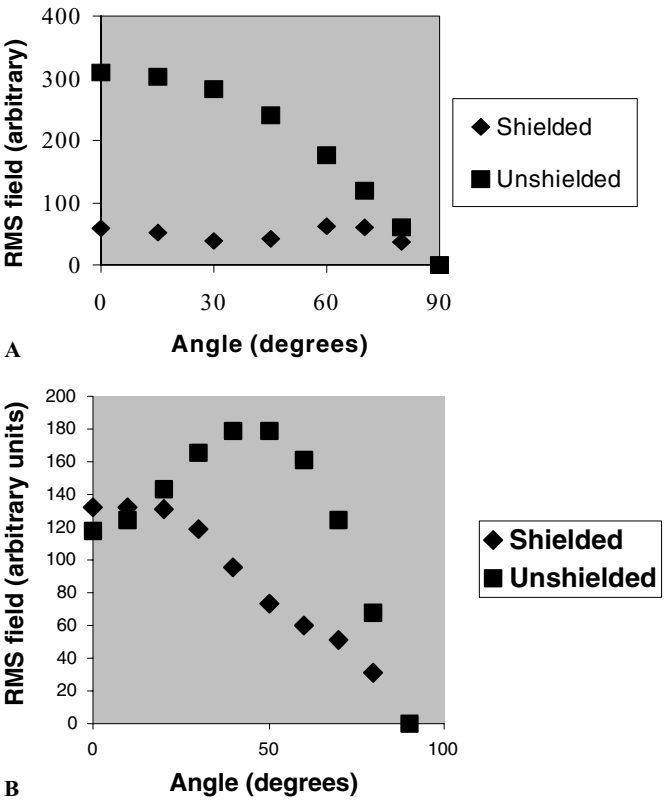

FIG. 6. (A) The shielding characteristic of the y-gradient. The z-component of the magnetic field was calculated at points 5 mm outside the return paths in angular increments. It shows that the one line calculation (amounting to the zero degree point in the figure) was effective for this gradient. (B) The shielding characteristic of the x-gradient at the same position, showing partial success for the shielding in this geometry.

for this gradient. For the x-gradient, the shielding only has an effect over part of the coil with the greatest reduction in the residual field occurring at approximately 45°, the position used in the algorithm. The characteristic is shown in Fig. 6B. Further improvements may require enhancements to the coil geometry.

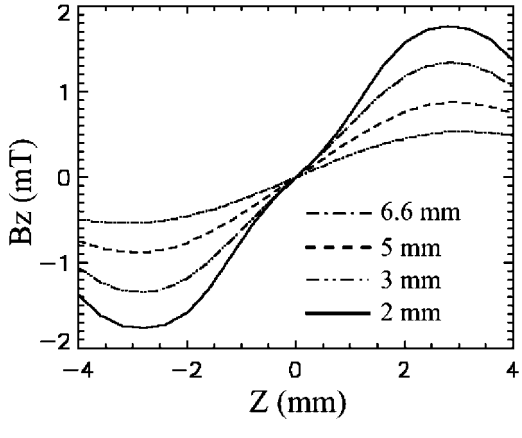

FIG. 7. B_z along the z-axis for different separations of the z-gradient coil.

It is noted that the distance between the coil halves could be adjusted somewhat and still provide a usable imaging region, leading to some leeway in the construction. So, it is possible that the coil halves may be placed as close as possible together in order to maximize gradient strength for a given sample. The calculated z-gradient strength increases from 274 to 590 mT/m/A if the distance between the planes is decreased from 6.6 to 3.6 mm, and in this particular case, the size of the linear region in the z-x plane increases. Plots of the calculated gradient strength along the z-axis are shown for the different plane separations in Fig. 7.

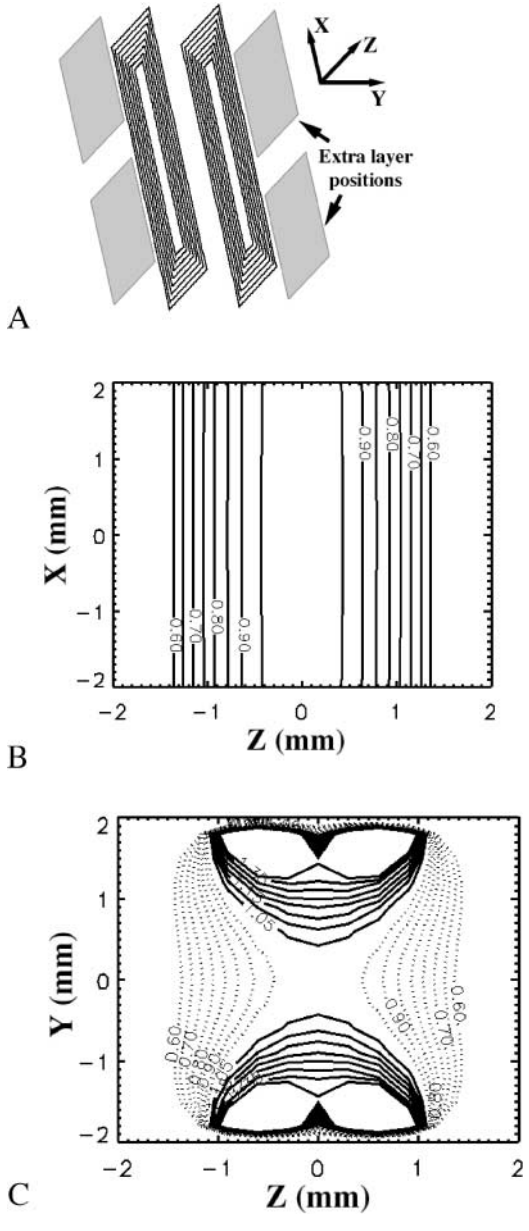

FIG. 8. (A) A z-gradient design without the concentric return paths. For display purposes only, possible positions of shield or torque reduction coils are shown, although not included in any calculation. (B) A contour plot of gradient uniformity in the x-z plane at 5% levels from the central value. (C) Gradient uniformity in the y-z plane.

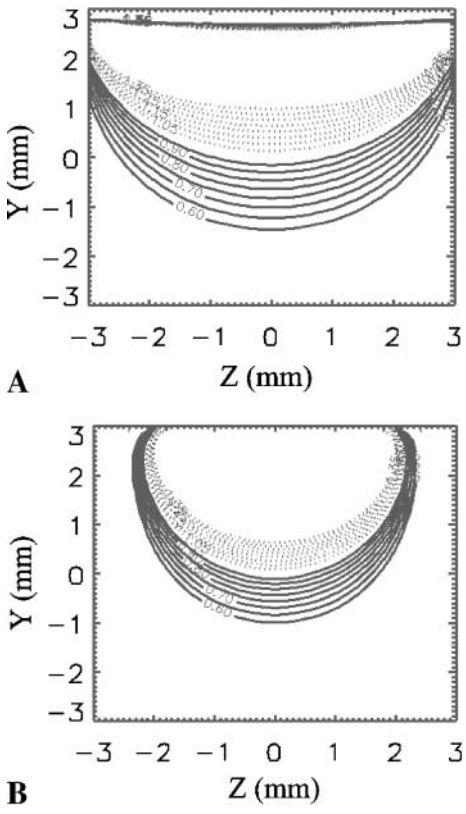

FIG. 9. Contour plot showing deviations in field linearity from the central value in the y-z plane for (A) a surface y-gradient; and (B) a surface z-gradient.

As mentioned previously, the z-gradient shielding does not work very well, becoming worse if the gradient halves are moved closer together. Indeed, the geometry of the z-gradient does not require the use of concentric return paths. The use of simple planar loops would appear to be most appropriate in this case as shown in Fig. 8A, with corresponding contour plots shown in Figs. 8B and 8C. This configuration also has a lower net torque of 4.3e-3 Nm/A on each half compared to 6.23e-3 Nm/A (at 7 T) for the configuration shown in Fig. 3. An extra layer may also be added between the x-gradient loops, for further enhancing the design with either torque reduction or with shielding, represented by the gray squares, although this is not included in the magnetic field calculations.

Surface Gradients

The possibility also exists of using only half of the constructed set, thus providing a set of surface gradients. Planes parallel to the x-z plane provide reasonable linear field regions, while those with a y-dependence can provide up to 200 μm within 5% of a chosen value. Figure 9 shows examples of gradient contour plots showing deviations from a chosen point in steps of 5% for a surface y-gradient in Fig. 9A and a surface z-gradient in Fig. 9B in the y-z plane. In the x-z plane, contour plots will be the same as shown previously for the biplanar set, but with half the gradient strength. Moving away from this plane, while remaining parallel to it, the natural falloff of gradient strength with distance from the coil will be observed. Although the gradient strength is reduced in this configuration, even easier access to the sample can be enabled, perhaps offsetting this disadvantage.

MR Methods

Two-dimensional MR images have been acquired using a 15-cm horizontal 7-T magnet equipped with a Bruker AVANCE console and using a gradient-echo sequence without slice selection, using the following parameters: TR/TE = 500/1.2 ms; flip angle (FA) = 45°. Similar parameters are used for 3D experiments. The scan time and resolution were dependent on the particular experiment. The echo maximum was acquired at 10% of the read gradient time, in order to reduce diffusion losses (*9*). Eddy currents were tested using a series of FID acquisitions after a gradient pulse. No eddy currents were observed at a 100-μs delay after the gradient using a maximum pulse current of 4 A and a risetime of 100 μs.

Biplanar Gradient Results

Prototype x- and z-biplanar gradient sets were built according to the design optimization algorithm with the x-gradient spacing set to 6 mm and the z-gradient to 5 mm. Two wire windings of 0.25-mm diameter (32 AWG) wire were placed at each position on a 20-mm diameter cylindrical former. The x-gradient is an unshielded design and the z-gradient is shielded, one-half of which is shown in Fig. 10. To construct the gradient, small

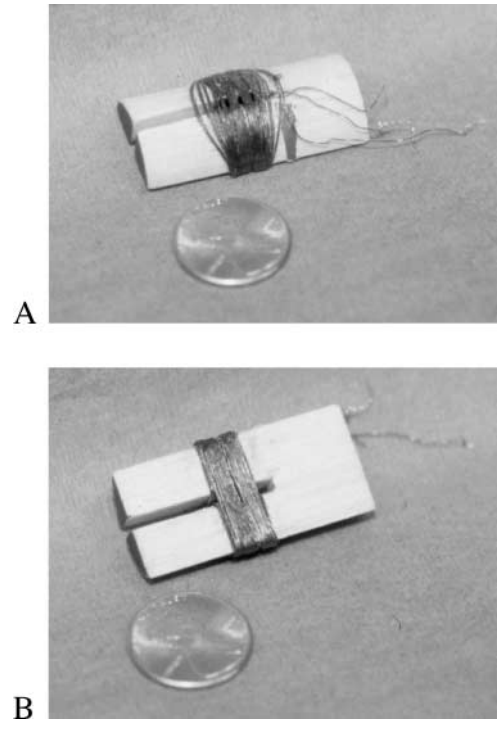

FIG. 10. Photographs (back and front) of one-half of the prototype x and z gradients, next to a 1.95-cm diameter coin.

notches were cut into the wooden former at critical positions (i.e., the azimuth of the return paths and the bends to the planar section of the coil). Initially, the wires were fastened with a cyanoacrylate glue, and after completion of both layers, was potted in epoxy. Struts were placed on either end of the gradient former for each half of the coil. The RF coil was placed on a 1-mm-thick board with a width of 3 cm. The struts on the gradient former were of the appropriate height on each half of the gradients such that when placed on the RF board, the sample was in the center and the distance between the gradient halves was 3 mm at the closest point. As the formers for each half were made from the same piece of material, they could be lined up in the z-direction with the aid of a straight board with a groove cut into it (to accommodate the RF assembly. The gradient and RF assembly was then placed into a small tube which fits tightly into a 4.5-cm diameter gradient set already in place. The resistance of the x-gradient was calculated to be 2.48 Ω and measured to be 2.6 ± 0.1 Ω. The resistance of the z-gradient was calculated to be 2.03 Ω and measured to be 2.1 ± 0.1 Ω. Inductances were 35 ± 2 μH and 54 ± 2 μH for the z- and x-gradients, respectively. These were measured with a Leader LCR-740 LCR bridge (Leader Instruments, USA) at 1 kHz.

Figure 11A shows an MR image of oil in the presence of a copper transmission electron microscopy (TEM) grid on which TEM samples are usually placed. It is used here as a convenient planar resolution phantom with eventual aim of comparing TEM images with MR images (*10*). The z-gradient strength was estimated to be 0.8 T m^{-1} with 0.4 A and the x-gradient strength

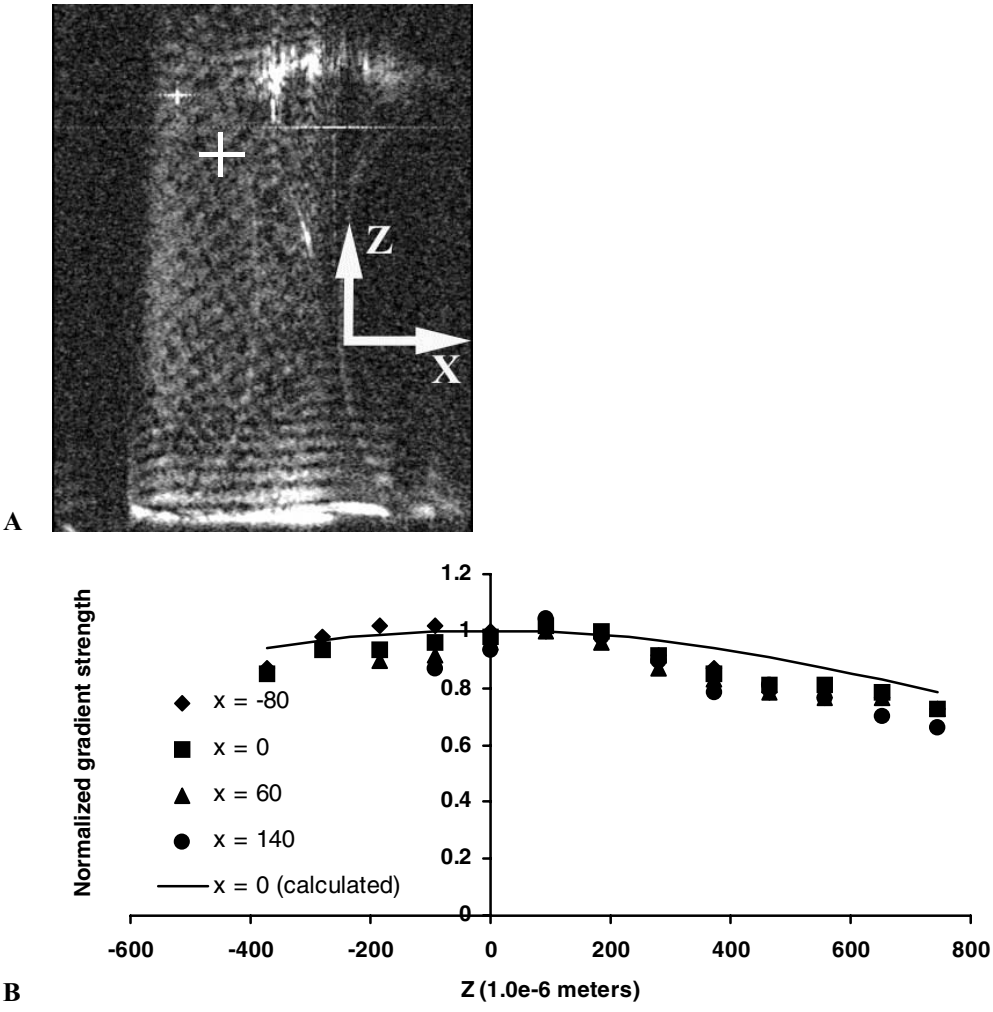

FIG. 11. (A) MR image of oil on a strip of copper in the presence of a 400-mesh copper TEM grid (bar spacing of 63 μm). The grid is seen to be resolved at a nominal resolution of 6 μm at the center (nominal resolution is defined here as grid spacing/number of pixels per grid section). The image foldback demonstrates the need for a small RF coil when using this arrangement. Image parameters were TR/TE = 500/1.2 ms; FA = 45°; matrix size = 512 × 130; scan time = 9 h; nominal in-plane resolution = 6 × 6 μm. The center pixel of the image is represented by the white square. Parts of the image with no signal have been cropped. (B) Using the grid in the image, the gradient strength across the image can be estimated. Measurements were performed by keeping a cursor over the image at a constant x-position and noting the z-coordinate at the grid crossing point.

was 0.7 T m^{-1} with 1 A. The grid used for the experiment was a 400-mesh grid (a bar spacing of 63 μm). There is some obvious foldback in the image, highlighting the need for a small RF coil. The grid, which forms in the image, may be used to provide a field map. The assumption is made that the dB/dz component produced by the x-gradient coil is small compared to that of the z-gradient. This is shown in Fig. 11B.

Surface Gradient Images

Both a two-axis (x and z) and a three-axis surface gradient set were built. The two-axis set consisted of an unshielded x-gradient with a simple loop structure for the z-gradient. For the two-axis set we show in Fig. 12 an image of a 300-mesh (bar spacing of 83 μm) TEM grid in oil. Again, distortion can be seen, although the center of the gradient provides usable imaging region. The maximum gradient strengths were estimated to be 0.5 T/m with 1.0 A for x and 0.6 T/m at 0.5 A for z, with the gradient placed approximately 1 mm from the sample. The resistance for the x-gradient was calculated to be 1.24 Ω and measured at 1.3 Ω. The resistance for the z-gradient was calculated to be 0.38 Ω and measured to be 0.4 Ω. The inductances were measured to be 8 ± 2 μH and 26 ± 2 μH for the z- and x-gradients, respectively, at 1 kHz.

For the 3-axis gradient set (the 2-axis set plus a shielded y-gradient design), we show sections from a 3D MR image of a 200-μm inner diameter tube of oil in Fig. 13. In this configuration, the gradient efficiencies were approximately 0.35 T/m/A for x, 0.9 T/m/A for the z-gradient, and 1.1 T/m/A for the y-gradient. The smaller values for the x- and z-gradients were due to the increased distance from the sample with y-gradient presence. The resistance of the y-gradient was calculated to be 1.14 Ω and measured at 1.2 Ω. The inductance was measure to be 25 ± 2 μH. Some small distortion is present, possibly because of slightly incorrect placement of the sample beneath the gradient coil. Any tapering effect due to the natural gradient strength is difficult to observe. The sample was at a slight angle to the gradient coil, and so the field of view rectangle is rotated in the images.

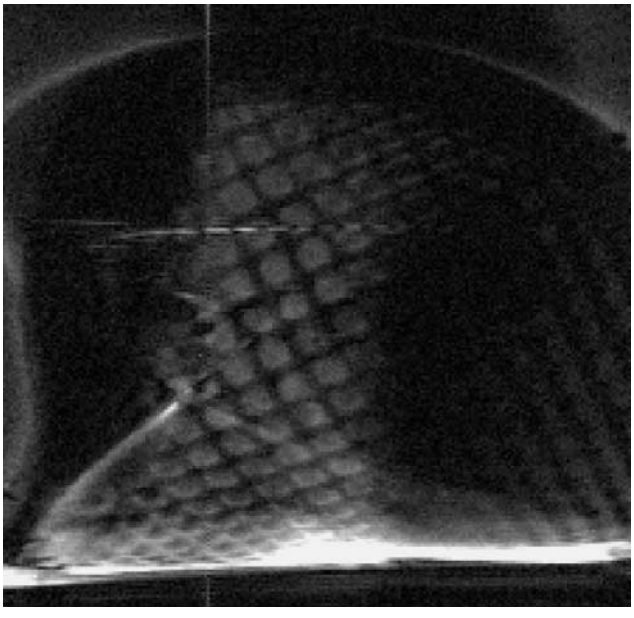

FIG. 12. MR image of oil around a 300-mesh (83 μm bar spacing) TEM grid. The imaging parameters were as before but with a matrix size of 256×130 (zero filled to 256×256), with a nominal resolution of 8 μm at the center.

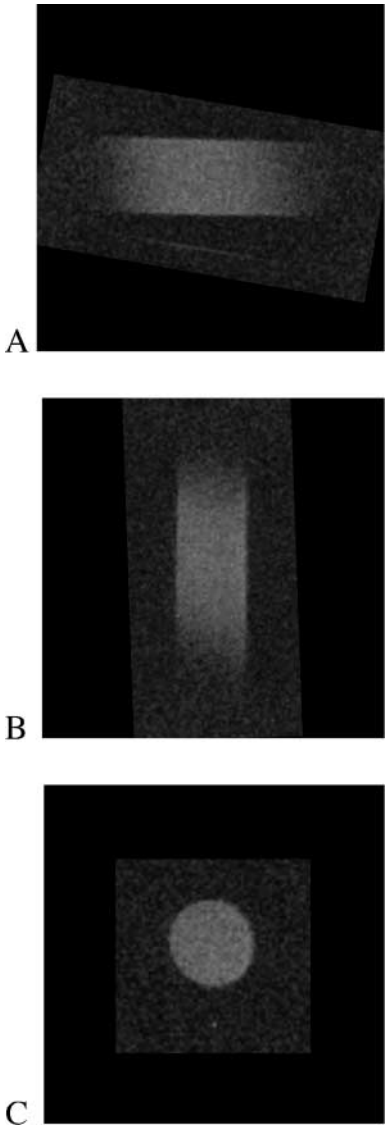

FIG. 13. Cross-sections of a 3D MR image of a 200-μm i.d. tube filled with oil, taken with the 3D surface coil gradient set. Image parameters were as before apart from a matrix size of $128 \times 64 \times 64$, nominal resolution of 7 μm isotropic, and scan time of 4.5 h with 8 averages.

DISCUSSION

The unique feature of the design methodology is that only the gradient strength at the origin of the coil is used to determine

the design. No attempt is made to increase the size of the gradient region with further constraints. This is reasonable given the sample size used in solenoidal RF microcoils. For planar samples, such as the TEM grids used here, care has to be taken to design appropriately small receivers in cases where the sample dimensions exceed the zero crossover points of the gradients.

The x-gradient strength per unit current is noted to be approximately half that of the other two gradients. This is compounded in this case by the necessity of having the x-gradient plane separation being the furthest away from the sample due to construction constraints and is noted here to be about one-third of the z-gradient strength. Adding relatively more windings to the x-gradient (compared to the y- or z-gradient) will also be appropriate, however, at the expense of the coil's impedance. The lower efficiency of the x-gradient is also noted in other planar designs for horizontal-bore magnets (*11*). This is due to not being able to place wires in a direction perpendicular to the x-direction and is a limitation to the design.

For small gradient sets, with small cross-section wires, the resistance of the coil increases dramatically (*12*). Again this is of particular importance for the x-gradient. If the figure of merit (efficiency)^2, resistance (*12*) is examined it is seen that the gradient configuration used in the biplanar experiment has the x-gradient being a factor of 10 worse than the z-gradient. In the surface gradient experiment (where the three gradients are used), this figure of merit for the x-gradient is only 8% of that for the y-gradient, the most efficient coil. Thermally conductive epoxy (*13*) along with a cooling system will become imperative for this system. The coolant path may be placed directly next to the x-gradient, an advantage in the construction of this coil.

As stated previously, no eddy currents have been observed at the gradient strengths used for the experiments. This is mainly due to the relatively large distance from any surrounding metal. Shielding benefits will be more obvious in smaller bore magnets. However, the spreading of the return paths is noted to significantly increase the calculated gradient strength for the x- and y-gradients and is reason enough to be employed. It is perhaps more accurate to say that the coils are overshielded in their straight return path position.

As noted previously, the symmetry of the z-gradient allows each coil half to be placed on a single plane, without the need for the concentric return paths, creating an improvement in the compactness of the z-gradient design and resulting in a lower fringe field. The torque is also reduced, but is still significant and may need to be corrected in order to address movement concerns. It is noted that having the z-gradient with return paths moving directly back such as in Fig. 5 results in a zero net torque. If an extra layer is added, for shielding or torque reduction, a possible configuration is shown in Fig. 6. Such a design has yet to be realized.

It is noted and expected that interactions between the gradients cause image distortions if the sample is placed incorrectly, particularly with the x-gradient. The small linear region requires sample placement accuracy of less than 1 mm, a difficult, but certainly not impossible, task to achieve. A greater challenge is presented by the construction of the RF coils; however, this is also reasonably possible.

One possible application for the surface gradient design is for use as part of a movable imaging probe, as was originally suggested by Cho and Yi (*14*) for their surface gradient design. The design presented here though is substantially more compact, and it is suggested that together with a small RF coil, it may be used to image planar samples, such as on a microscope slide, with the sample or the probe being moved to focus on a particular section in a similar manner as a light microscope.

In conclusion, a design for a three-axis gradient set with a planar section for the gradient generation and concentric return paths has been presented. Prototype biplanar and surface gradients were built and tested, providing high-resolution MR images with small RF coils.

ACKNOWLEDGMENTS

Preliminary results describing this work were presented at the 5th International Conference for Magnetic Resonance Microscopy held in September 1999, in Heidelberg, Germany. We thank Dr. Donald S. Williams for helpful discussions. The work is supported by research grants from the National Institutes of Health (R01RR-10962 and R01RR/AI-15187) and The Whitaker Foundation. The experiments were performed in the Pittsburgh NMR Center for Biomedical Research, which is supported by a Grant (P41RR-03631) from the National Center for Research Resources as a National Institutes of Health-supported Resource Center.

REFERENCES

1. P. T. Callaghan, M. E. Komlosh, and M. Nyden, *J. Magn. Reson.* **133,** 177 (1998).
2. R. Bowtell and A. Peters, *Magn. Reson. Med.* **41,** 600 (1999).
3. W. W. Brey, T. H. Mareci, and J. Dougherty, *J. Magn. Reson. B* **112,** 124 (1996).
4. F. D. Doty and J. K. Wilcher, U.S. Patent 5,554,929, crescent gradient coils, 1996.
5. T. L. Peck, R. L. Magin, and P. C. Lauterbur, *J. Magn. Reson. B* **108,** 114 (1995).
6. J. E. Stocker, T. L. Peck, A. G. Webb, M. Feng, and R. L. Magin, *IEEE Trans. Biomed. Eng.* **44,** 1122 (1997).
7. D. A. Seeber, J. H. Hoftiezer, W. B. Daniel, M. A. Rutgers, and C. H. Pennington, *Rev. Sci. Instrum.* **71,** 4263 (2000).
8. S. Crozier and D. M. Doddrell, *J. Magn. Reson. A* **103,** 354 (1993).
9. Z. H. Cho, C. B. Ahn, S. C. Juh, H. K. Lee, R. E. Jacobs, S. Lee, J. H. Yi, and J. M. Jo, *Med. Phys.* **15,** 815 (1988).
10. S. J. Dodd, M. Williams, J. Suhan, D. S. Williams, A. P. Koretsky, and C. Ho, *in* "Proceedings, ISMRM 7th Scientific Meeting, Philadelphia, May 22–28, 1999," p. 2126.
11. M. A. Martens, L. S. Petropoulos, R. W. Brown, J. H. Andrew, M. A. Morich, and J. L. Patrick, *Rev. Sci. Instrum.* **62,** 2639 (1991).
12. R. Bowtell and P. Robyr, *J. Magn. Reson.* **131,** 286 (1988).
13. S.-C. Lee, K. Kim, J. Kim, S. Lee, J. H. Yi, S. W. Kim, K.-S. Ha, and C. Cheong, *J. Magn. Reson.* **150,** 207 (2001).
14. Z. H. Cho and J. H. Yi, *J. Magn. Reson.* **94,** 471 (1991).